Journal of Sound and Vibration (2000) **234**(5), 799–817
doi:10.1006/jsvi.1999.2896, available online at http://www.idealibrary.com on IDEAL®

NON-LINEAR VIBRATION ABSORBERS USING HIGHER ORDER INTERNAL RESONANCES

P. Frank Pai and Bernd Rommel

Mechanical and Aerospace Engineering Department, University of Missouri, Columbia, MO 65211, U.S.A.

AND

Mark J. Schulz

Mechanical Engineering Department, North Carolina A&T State University, Greensboro, NC 27411, U.S.A.

(*Received* 30 *June* 1999, *and in final form* 27 *December* 1999)

This paper presents a study of controlling steady-state vibrations of a cantilevered skew aluminum plate using saturation phenomena due to higher-order internal resonances. PZT (lead zirconate titanate) patches are used as control actuators and sensors. Linear second order controllers are designed to couple with the plate via different orders of non-linear terms to establish energy bridges between the plate and controllers. Each linear second-order controller is designed to have a 1 : 2 or 1 : 3 or 1 : 4 internal resonance with one of the plate's vibration modes and hence is able to exchange energy with the plate around the specific modal frequency. Because of non-linearities and internal resonances, different orders of saturation phenomena exist and are used to suppress modal vibrations. Several non-linear vibration absorbers are designed based on the saturation phenomena and are analyzed to show their feasibility and efficiency. Perturbation analysis, direct numerical integration, and experiments are performed to validate these non-linear vibration absorbers.

1. INTRODUCTION

For a weakly non-linear system with quadratic non-linearities and 1 : 2 internal resonance between two linear natural frequencies, a saturation phenomenon exists [1]. This 1 : 2 internal resonance and the corresponding 1 : 2 saturation phenomenon have been used to design non-linear controllers [2–8]. These control techniques use a linear second-order controller coupled to a linear vibration system via quadratic terms. These quadratic terms establish a channel for energy exchange between the system and the controller, resulting in a beating phenomenon in the response of the combined system. For controlling transient vibrations, the beating phenomenon is used to channel energy from the system to the controller and then the energy is dissipated by adding dampings to the controller before it has the opportunity to revert back to the system [7]. For controlling steady-state vibrations, the quadratic term on the system results in a resisting force against the external excitation force to suppress vibrations [7]. Because there is no decision making required in such saturation controllers, it does not need a computer to compute the required control force for control actuators. Hence, saturation controllers can be built using simple off-shelf electronic circuits [3, 6] and can be used to regulate dynamical systems to prevent severe resonant vibrations [2].

0022-460X/00/300799 + 19 $35.00/0

This work is to design new non-linear vibration absorbers using higher-order internal resonances and saturation phenomena to suppress the steady-state vibrations of a cantilevered skew aluminum plate. Higher-order internal resonances are introduced by using quadratic, cubic, and/or quartic terms to couple the controller with the plate. PZT patches are used for control actuation and sensing, and displacement and velocity feedback signals are considered. Perturbation analysis is used to predict the dynamic response, and direct numerical integration and experiments are performed to verify the analytical prediction and to validate the designs.

2. 1:2 NON-LINEAR VIBRATION ABSORBER

The 1:2 non-linear vibration absorber for suppressing structural vibrations can be described by the following two ordinary differential equations [1, 7]:

$$\ddot{u}_1 + 2\zeta_1\omega_1\dot{u}_1 + \omega_1^2 u_1 = g_{12}u_1u_2, \qquad \ddot{u}_2 + 2\zeta_2\omega_2\dot{u}_2 + \omega_2^2 u_2 = g_{11}u_1^2 + F\cos(\Omega t), \tag{1}$$

where u_1 denotes the response of a second-order controller, ω_1 is the natural angular frequency of the controller, ζ_1 is the damping ratio of the controller, u_2 represents one of the modal co-ordinates of a structure, ω_2 is the modal frequency, ζ_2 is the modal damping ratio, $g_{11}$and g_{12} are positive gain constants, F is the amplitude of the external excitation force, Ω is the external excitation frequency, ω_2 is close to $2\omega_1$, Ω is close to ω_2, t is the time, and $(\dot{}) \equiv \mathrm{d}(\,)/\mathrm{d}t$. The structural vibration is assumed to be linear, but the structure becomes part of a larger non-linear system when it is coupled with the controller. Because the controller is responsible for the desirable non-linear characteristics of the larger system, non-linear tailoring of the system is relatively straightforward and easy.

To test different non-linear vibration absorbers, we built a digital control system that consists of SIMULINK modelling software[†] and a dSPACE DS1102 controller system[‡] in a pentium computer. This system is described in detail in reference [7]. Figure 1 shows the geometry and dimensions of the cantilevered skew aluminum plate under study with three integrated PZT (lead zirconate titanate) patches and a 1:2 non-linear vibration absorber for controlling the first-mode vibration using this digital control system. The aluminum plate has Young's modulus 10×10^6 psi, the Poisson ratio 0·3, mass density $2{\cdot}54\times10^{-4}$ lb·s^2/in^4, and thickness 0·122 in. The PZT patches are one QP10N and two QP10W QuickPack PZT actuators purchased from ACX.[§] The size of QP10N in $2''\times1''\times0{\cdot}015''$, and its piezo-wafer size is $1{\cdot}81''\times0{\cdot}81''\times0{\cdot}010''$. The size of QP10W is $2''\times1{\cdot}5''\times0{\cdot}015''$, and its piezo-wafer size is $1{\cdot}81''\times1{\cdot}31''\times0{\cdot}010''$. One of the two QP10W patches is used for control actuation, and the other QP10W is placed on the backside but the same location of the plate and is used to provide the assumed external excitation. The QP10N patch is used as a sensor.

To know the dynamic characteristics of the plate we perform finite element analyses using an in-house finite element code GESA [9], and we also use a Polytec PI PSV-200 Scanning Laser Vibrometer (SLV) to obtain frequency response functions (FRFs), natural frequencies, and operational deflection shapes (ODSs) [10]. The first three natural frequencies are obtained to be 13·4, 66·4, and 77·1 Hz, and the first three modal damping

[†] The MathWorks, Inc. Natick, MA.
[‡] dSPACE digital processing and control engineering GmbH, Paderborn, Germany.
[§] Active Control eXperts, Inc., Cambridge, MA.

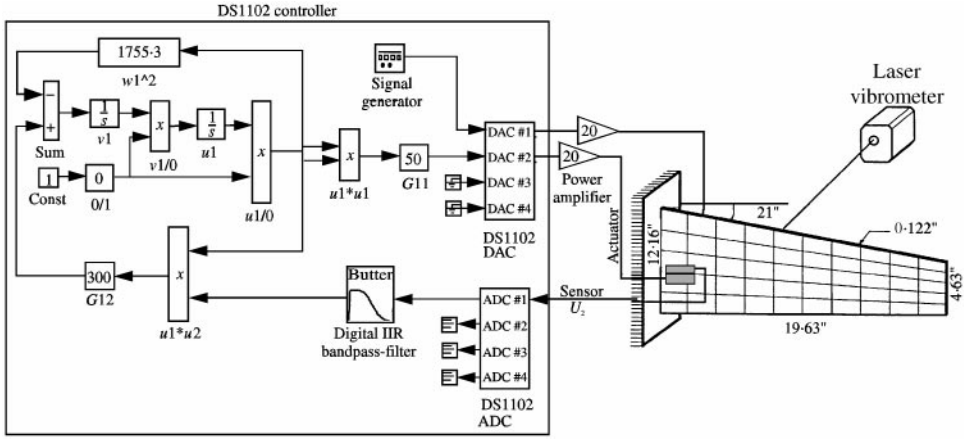

Figure 1. The cantilevered skew aluminium plate with a 1 : 2 non-linear vibration absorber for controlling the first-mode vibration.

ratios are 0·306, 0·085 and 0·047%. Because of non-rectangular geometry, all modes are bending-torsional vibrations, even the first mode.

The g_{12} in equation (1) is exactly the same as the gain constant $G12$ in the DS1102 controller in Figure 1. On the other hand, the actual excitation voltage $\hat{F} * \cos(\Omega t)$ to the external excitation PZT actuator and the actual excitation voltage $G11 * u1 * u1 * 20$ to the controlling PZT actuator are indirect excitation voltages to u_2. When u_2 is not coupled with u_1 (i.e., $g_{11} = g_{12} = 0$): if a voltage $\hat{F} \cos \Omega t$ is applied to the external actuator and the response amplitude of u_2 is measured to be a_2, it follows from the linear vibration theory that the direct excitation voltage F to the PZT sensor is

$$F = a_2 \omega_2^2 \sqrt{\left(1 - \frac{\Omega^2}{\omega_2^2}\right)^2 + \left(2\zeta_2 \frac{\Omega}{\omega_2}\right)^2}. \tag{2}$$

Then g_{11} can be obtained as

$$g_{11} = G11 \times 10 \times 20 = 200 \times G11, \tag{3}$$

where the 20 accounts for the use of a power amplifier. An input voltage to the A/D channels of the dSPACE board is scaled by a factor of 1/10. Moreover, before a signal is sent to the D/A channels of the dSPACE board, it is multiplied by a factor of 10. The 10 in equation (3) accounts for this fact. However, it has been observed that, if PZT patches are connected to the input channels of the DSP board, the scaling factor is not exactly equal to 1/10. If the voltage generated by a PZT patch is measured using an oscilloscope, the value is different from the value measured using the DSP board by a factor other than 10. This phenomenon exists only when the PZT patch is directly connected to the DSP board. To solve this problem requires a signal conditioning circuit designed to separate the RC circuit of the PZT sensor from the DSP board, which is beyond the scope of this research. Instead of designing a signal conditioner we obtain the scaling factor appropriate for the PZT patch when it is directly connected to the DSP board.

We excite the structure with an excitation amplitude $\hat{F} = 10$ V at the first modal frequency. We then measure the response amplitude of the PZT sensor using an

oscilloscope and the DSP board to find the scaling factor to be 10·85 for the first-mode vibration. Moreover, the amplitude of the output voltage of the PZT sensor is measured to be $a_2 = 0{\cdot}186 \times 10{\cdot}85 = 2{\cdot}02$ V, when $\hat{F} = 10$ V and the excitation frequency Ω is equal to the first natural frequency. From equation (2) we obtain that $F = 86{\cdot}71$ V/s^2 and $F/\hat{F} = 8{\cdot}67\ 1/s^2$. Hence, it follows from Figure 1 that the system equations for the control of the first-mode steady-state vibration are

$$\ddot{u}_1 + \omega_1^2 u_1 = G12 \times u_1 u_2,$$

$$10{\cdot}85(\ddot{u}_2 + 0{\cdot}5028\dot{u}_2 + 7021u_2) = \frac{F}{\hat{F}}[G11 \times 200u_1^2 + \hat{F}\cos(\Omega t)]. \tag{4}$$

u_1 is the controller voltage inside the DS1102 controller, u_2 is the sensor voltage inside the DS1102, and $10{\cdot}85u_2$ is the actual sensor voltage. In equation (4), $\zeta_1 = 0$ is used. Moreover, we use the fact that the PZT patch for external excitation and the PZT patch for control have the same size and are located at the same position and hence they have the same $F/\hat{F}$. The same procedure can be used to derive the system equations for the control of other modes.

Numerical and experimental results show that the 1 : 2 non-linear vibration absorber works well and it is robust and efficient in controlling steady-state vibrations around resonance areas of structures [7, 10]. Here we are interested in using the uncovered working mechanism of the 1 : 2 non-linear vibration absorber to design and verify new non-linear vibration absorbers using higher-order non-linearities and the corresponding internal resonances and saturation phenomena.

3. 1 : 2 : 4 NON-LINEAR VIBRATION ABSORBER

To show the use of higher-order internal resonances and saturation phenomena for structural vibration control, we consider the following three ordinary differential equations:

$$\ddot{u}_1 + 2\xi_1\omega_1\dot{u}_1 + \omega_1^2 u_1 = \bar{g}_{124}u_1\dot{u}_2\dot{u}_4, \qquad \ddot{u}_2 + 2\xi_2\omega_2\dot{u}_2 + \omega_2^2 u_2 = \bar{g}_{24}\dot{u}_2\dot{u}_4,$$

$$\ddot{u}_4 + 2\xi_4\omega_4\dot{u}_4 + \omega_4^2 u_4 = \bar{g}_1 u_1^2\dot{u}_1^2 + \bar{g}_2 u_2^2 + \bar{F}\cos(\Omega t), \tag{5}$$

where u_1 denotes the response of one of the two second-order controllers, ω_1 is its natural angular frequency, and ξ_1 is its damping ratio. u_2 denotes the response of the other second-order controller, ω_2 is its natural angular frequency, and ξ_2 is its damping ratio. Moreover, u_4 represents one of the modal co-ordinates of a structure, ω_4 is the modal frequency, ξ_4 is the modal damping ratio, $\bar{g}_2$ and $\bar{g}_{24}$ are positive gain constants, $\bar{g}_1$ and $\bar{g}_{124}$ are positive or negative gain constants, $\bar{F}$ is the amplitude of the external excitation force, Ω is the external excitation frequency, Ω is close to ω_4, ω_4 is close to $2\omega_2$, ω_4 is close to $4\omega_1$, t is the time, and $(\dot{}) \equiv \mathrm{d}(\,)/\mathrm{d}t$. The design of this 1 : 2 : 4 non-linear vibration absorber was determined after we studied several higher-order non-linear vibration absorbers. Some of those vibration absorbers deserve attention and are shown later in section 5.

3.1. PERTURBATION ANALYSIS

We seek a first-order approximate solution of equation (5) by using the method of multiple scales [1] in the form

$$u_1(T_0, T_1; \varepsilon) = u_{10}(T_0, T_1) + \varepsilon u_{11}(T_0, T_1) + \cdots,$$

$$u_2(T_0, T_1; \varepsilon) = u_{20}(T_0, T_1) + \varepsilon u_{21}(T_0, T_1) + \cdots,$$

$$u_4(T_0, T_1; \varepsilon) = u_{40}(T_0, T_1) + \varepsilon u_{41}(T_0, T_1) + \cdots. \tag{6}$$

where ε is a small dimensionless parameter used for book-keeping only; $T_0 = t$, a fast scale characterizing motions at Ω and its multiplies; and $T_1 = \varepsilon t$, a slow scale characterizing the time variation of the amplitudes and phases. To make dampings, non-linearities, and the primary resonance force appear in the same perturbation equations, we order that $\bar{F} = \varepsilon F$, $\xi_1 = \varepsilon\zeta_1$, $\xi_2 = \varepsilon\zeta_2$, $\xi_4 = \varepsilon\zeta_4$, $\bar{g}_1 = \varepsilon g_1$, $\bar{g}_2 = \varepsilon g_2$, $\bar{g}_{124} = \varepsilon g_{124}$, and $\bar{g}_{24} = \varepsilon g_{24}$. Although the method of multiple scales is well known in the literature, the combination of the four non-linearities in equation (5) and the ordering scheme used has not been studied by other researchers. Hence, we show below some steps of the perturbation analysis using the method of multiple scales.

Substituting equation (6) into equation (5) and equating coefficients of like powers of ε, we obtain the following:

Order ε^0:

$$D_0^2 u_{10} + \omega_1^2 u_{10} = 0, \qquad D_0^2 u_{20} + \omega_2^2 u_{20} = 0, \qquad D_0^2 u_{40} + \omega_4^2 u_{40} = 0. \tag{7}$$

Order ε:

$$D_0^2 u_{11} + \omega_1^2 u_{11} = -2D_0(D_1 u_{10} + \zeta_1\omega_1 u_{10}) + g_{124} u_{10}(D_0 u_{20})(D_0 u_{40}),$$

$$D_0^2 u_{21} + \omega_2^2 u_{21} = -2D_0(D_1 u_{20} + \zeta_2\omega_2 u_{20}) + g_{24}(D_0 u_{20})(D_0 u_{40}),$$

$$D_0^2 u_{41} + \omega_4^2 u_{41} = -2D_0(D_1 u_{40} + \zeta_4\omega_4 u_{40}) + g_2 u_{20}^2 + g_1 u_{10}^2 (D_0 u_{10})^2 + F\cos(\Omega T_0), \tag{8}$$

where $D_0 \equiv \partial/\partial T_0$ and $D_1 \equiv \partial/\partial T_1$. The solutions of equation (7) can be expressed in the form

$$u_{10} = A_1(T_1)\mathrm{e}^{\mathrm{i}\omega_1 T_0} + \mathrm{cc}, \qquad u_{20} = A_2(T_1)\mathrm{e}^{\mathrm{i}\omega_2 T_0} + \mathrm{cc}, \qquad u_{40} = A_4(T_1)\mathrm{e}^{\mathrm{i}\omega_4 T_0} + \mathrm{cc}, \tag{9}$$

where A_1, A_2, and A_4 are arbitrary functions at this level of approximations, $\mathrm{i} \equiv \sqrt{-1}$, and cc denotes complex conjugate terms. Substituting equation (9) into equation (8) yields

$$D_0^2 u_{11} + \omega_1^2 u_{11} = -2\mathrm{i}\omega_1(A_1' + \zeta_1\omega_1 A_1)\mathrm{e}^{\mathrm{i}\omega_1 T_0} + g_{124}\omega_2\omega_4 \bar{A}_1 \bar{A}_2 A_4 \mathrm{e}^{\mathrm{i}(\omega_4 - \omega_1 - \omega_2)T_0} + \mathrm{NST} + \mathrm{cc},$$

$$D_0^2 u_{21} + \omega_2^2 u_{21} = -2\mathrm{i}\omega_2(A_2' + \zeta_2\omega_2 A_2)\mathrm{e}^{\mathrm{i}\omega_2 T_0} + g_{24}\omega_2\omega_4 \bar{A}_2 A_4 \mathrm{e}^{\mathrm{i}(\omega_4 - \omega_2)T_0} + \mathrm{NST} + \mathrm{cc},$$

$$D_0^2 u_{41} + \omega_4^2 u_{41} = -2\mathrm{i}\omega_4(A_4' + \zeta_4\omega_4 A_4)\mathrm{e}^{\mathrm{i}\omega_4 T_0} - g_1\omega_1^2 A_1^4 \mathrm{e}^{\mathrm{i}4\omega_1 T_0} + g_2 A_2^2 \mathrm{e}^{\mathrm{i}2\omega_2 T_0}$$

$$+ \tfrac{1}{2} F\mathrm{e}^{\mathrm{i}\Omega T_0} + \mathrm{NST} + \mathrm{cc}, \tag{10}$$

where $(\,)' \equiv \partial(\,)/\partial T_1$ and NST denotes non-secular terms. Three detuning parameters σ_1, σ_2, and σ_3 are introduced below as

$$\varepsilon\sigma_1 \equiv \Omega - \omega_4, \qquad \varepsilon\sigma_2 \equiv 2\omega_2 - \omega_4, \qquad \varepsilon\sigma_3 \equiv 2\omega_1 - \omega_2. \tag{11}$$

Substituting equation (11) into equation (10) and setting the coefficients of the secular terms [1] to zero yields the solvability conditions as

$$-2\mathrm{i}\omega_1(A_1' + \zeta_1\omega_1 A_1) + g_{124}\omega_2\omega_4\bar{A}_1\bar{A}_2A_4\mathrm{e}^{-\mathrm{i}(\sigma_2+\sigma_3)T_1} = 0,$$

$$-2\mathrm{i}\omega_2(A_2' + \zeta_2\omega_2 A_2) + g_{24}\omega_2\omega_4\bar{A}_2A_4\mathrm{e}^{-\mathrm{i}\sigma_2T_1} = 0,$$

$$-2\mathrm{i}\omega_4(A_4' + \zeta_4\omega_4 A_4) - g_1\omega_1^2A_1^4\mathrm{e}^{\mathrm{i}(\sigma_2+2\sigma_3)T_1} + g_2A_2^2\mathrm{e}^{\mathrm{i}\sigma_2T_1} + \tfrac{1}{2}F\mathrm{e}^{\mathrm{i}\sigma_1T_1} = 0. \tag{12}$$

Introducing polar notation $A_n(T_1) = \frac{1}{2}a_n(T_1)\,\mathrm{e}^{\mathrm{i}\theta_n(T_1)}$ into equation (12) and then setting the coefficients of the real and imaginary parts to zero yields the modulation equations

$$a_1' = -\omega_1\zeta_1a_1 + \frac{g_{124}\omega_2\omega_4}{8\omega_1}a_1a_2a_4\sin\phi_4, \tag{13}$$

$$\frac{\phi_1' - \phi_2' + 2\phi_4'}{4}a_1 = \frac{\sigma_1 - \sigma_2 - 2\sigma_3}{4}a_1 + \frac{g_{124}\omega_2\omega_4}{4\omega_1}a_1a_2a_4\cos\phi_4, \tag{14}$$

$$a_2' = -\omega_2\zeta_2a_2 + \frac{g_{24}\omega_4}{4}a_2a_4\sin\phi_2, \tag{15}$$

$$\frac{\phi_1' + \phi_2'}{2}a_2 = \frac{\sigma_1 - \sigma_2}{2}a_2 + \frac{g_{24}\omega_4}{4}a_2a_4\cos\phi_2, \tag{16}$$

$$a_4' = -\omega_4\zeta_4a_4 - \frac{g_2}{4\omega_4}a_2^2\sin\phi_2 - \frac{g_1\omega_1^2}{16\omega_4}a_1^4\sin(\phi_2 - 2\phi_4) + \frac{F}{2\omega_4}\sin\phi_1, \tag{17}$$

$$\phi_1'a_4 = \sigma_1a_4 + \frac{g_2}{4\omega_4}a_2^2\cos\phi_2 - \frac{g_1\omega_1^2}{16\omega_4}a_1^4\cos(\phi_2 - 2\phi_4) + \frac{F}{2\omega_4}\cos\phi_1, \tag{18}$$

where

$$\phi_1 \equiv \sigma_1T_1 - \theta_4, \qquad \phi_2 \equiv \theta_4 - 2\theta_2 - \sigma_2T_1, \qquad \phi_4 \equiv \theta_4 - 2\theta_1 - \theta_2 - (\sigma_2+\sigma_3)T_1. \tag{19}$$

The steady-state solutions correspond to constant a_i and ϕ_i, that is, $a_i' = \phi_i' = 0$. When $a_1 = 0$ and $a_2 = 0$, it follows from equations (17) and (18) that

$$a_4 = \frac{F}{2\omega_4\sqrt{\sigma_1^2 + \omega_4^2\zeta_4^2}}. \tag{20}$$

It is the linear forced response. Moreover, equations (13) and (14) show that, if $a_2 = 0$, $a_1 = 0$ and it corresponds to the linear solution.

If $a_1 \neq 0$, it follows from equations (13) and (14) that

$$a_2a_4 = \frac{8\omega_1}{|g_{124}|\omega_2\omega_4}\sqrt{(\omega_1\zeta_1)^2 + (\omega_1 - \Omega/4)^2}, \qquad \phi_4 = \tan^{-1}\frac{\zeta_1\omega_1}{\omega_1 - \Omega/4}. \tag{21}$$

If $a_2 \neq 0$, it follows from equations (15) and (16) that

$$a_4 = \frac{4}{g_{24}\omega_4}\sqrt{(\omega_2\zeta_2)^2 + (\omega_2 - \Omega/2)^2}, \qquad \phi_2 = \tan^{-1}\frac{\zeta_2\omega_2}{\omega_2 - \Omega/2}. \tag{22}$$

Moreover, it follows from equations (17) and (18) that

$$a_1 = \left(\frac{-b \pm \sqrt{b^2 - 4ac}}{2a}\right)^{1/4}, \tag{23}$$

where

$$a = \left(\frac{g_1\omega_1^2}{16\omega_4}\right)^2, \qquad b = \frac{g_1\omega_1^2}{8\omega_4}[C_1\sin(\phi_2 - 2\phi_4) - C_2\cos(\phi_2 - 2\phi_4)],$$

$$c = C_1^2 + C_2^2 - \frac{F^2}{4\omega_4^2}, \qquad C_1 \equiv \omega_4\zeta_4 a_4 + \frac{g_2}{4\omega_4}a_2^2\sin\phi_2,$$

$$C_2 \equiv \sigma_1 a_4 + \frac{g_2}{4\omega_4}a_2^2\cos\phi_2. \tag{24}$$

Equation (22) shows that $a_4 = 0$ if $\zeta_2 = 0$ and $\Omega = 2\omega_2$. In other words, even if the excitation is not at resonance (i.e., $\sigma_1 \neq 0$), a_4 still can be controlled to be zero if $\Omega = 2\omega_2$. Since the natural frequency ω_2 of the controller can be easily adjusted, theoretically this control method should also work for non-resonant situations. However, the perturbation solution is an approximation, and the actual solution may not behave so, especially outside of the resonance area.

Equation (22) shows that $a_4 = 0$ if $\zeta_2 = \Omega - 2\omega_2 = 0$, and equation (21) shows that $a_2 \to \infty$ if $a_4 = 0$ and $\zeta_1 \neq 0$ and/or $\Omega - 4\omega_1 \neq 0$. Moreover, if $\zeta_2 = \Omega - 2\omega_2 = 0$ and $\zeta_1 = \Omega - 4\omega_1 = 0$, a_2 is undetermined and the steady-state value of a_2 will depend on initial conditions, which are determined by the time that the controllers are activated. Again these are just predictions from the perturbation analysis and they need to be verified experimentally.

After the fixed-point solution is obtained by solving equations (13)–(18) with $a_i' = \phi_i' = 0$, the first-order approximate solution is obtained from equations (9), (11), and (19) to be

$$u_1 = u_{10} = a_1\cos\left(\frac{\Omega t}{4} - \frac{\phi_1 - \phi_2 + 2\phi_4}{4}\right),$$

$$u_2 = u_{20} = a_2\cos\left(\frac{\Omega t}{2} - \frac{\phi_1 + \phi_2}{2}\right), \qquad u_4 = u_{40} = a_4\cos(\Omega t - \phi_1). \tag{25}$$

3.2. STABILITY ANALYSIS

To determine the stability of linear and non-linear fixed-point solutions of equations (13)–(18), we introduce the Cartesian co-ordinates p_j and q_j as

$$p_1 = a_1 \cos\left(\frac{\phi_1 - \phi_2 + 2\phi_4}{4}\right), \qquad p_2 = a_2 \cos\left(\frac{\phi_1 + \phi_2}{2}\right), \qquad p_4 = a_4 \cos(\phi_1),$$

$$q_1 = a_1 \sin\left(\frac{\phi_1 - \phi_2 + 2\phi_4}{4}\right), \qquad q_2 = a_2 \sin\left(\frac{\phi_1 + \phi_2}{2}\right), \qquad q_4 = a_4 \sin(\phi_1). \tag{26}$$

Using equation (26) we reform equations (13)–(18) into

$$p_1' = -\omega_1\zeta_1 p_1 - \frac{\sigma_1 - \sigma_2 - 2\sigma_3}{4} q_1 + \frac{g_{124}\omega_2\omega_4}{8\omega_1}[p_4(q_1p_2 + p_1q_2) - q_4(p_1p_2 - q_1q_2)],$$

$$q_1' = -\omega_1\zeta_1 q_1 + \frac{\sigma_1 - \sigma_2 - 2\sigma_3}{4} p_1 + \frac{g_{124}\omega_2\omega_4}{8\omega_1}[p_4(p_1p_2 - q_1q_2) + q_4(q_1p_2 + p_1q_2)],$$

$$p_2' = -\omega_2\zeta_2 p_2 - \frac{\sigma_1 - \sigma_2}{2} q_2 + \frac{g_{24}\omega_4}{4}(q_2p_4 - p_2q_4),$$

$$q_2' = -\omega_2\zeta_2 q_2 + \frac{\sigma_1 - \sigma_2}{2} p_2 + \frac{g_{24}\omega_4}{4}(p_2p_4 + q_2q_4),$$

$$p_4' = -\omega_4\zeta_4 p_4 - \sigma_1 q_4 - \frac{g_2}{2\omega_4} p_2q_2 + \frac{g_1\omega_1^2}{4\omega_4}(p_1^3q_1 - p_1q_1^3),$$

$$q_4' = -\omega_4\zeta_4 q_4 + \sigma_1 p_4 + \frac{g_2}{4\omega_4}(p_2^2 - q_2^2) - \frac{g_1\omega_1^2}{16\omega_4}(p_1^4 - 6p_1^2q_1^2 + q_1^4) + \frac{F}{2\omega_4}. \tag{27}$$

Because these are first-order autonomous ordinary-differential equations, the stability of a particular fixed point with respect to an infinitesimal disturbance proportional to $e^{\lambda t}$ is determined by the eigenvalues of the Jacobian matrix of the right-hand sides of equation (27). A given fixed point is stable if and only if the real parts of all eigenvalues are less than or equal to zero. If there is a pair of complex conjugate values having positive real parts, amplitude- and phase-modulated motions are expected [11].

The main interest of this work is to design and investigate the feasibility and efficiency of new saturation controllers using higher-order internal resonances. Numerical and experimental bifurcation and stability analysis of the new saturation controllers are still under study because they require more efforts and time. As explained in section 2, the RC circuit of the PZT sensor is coupled with the DSP board, and hence the stability is affected by the circuit of the DSP board, which is a challenging problem to be solved.

3.3. SATURATION PHENOMENON

Equation (22) shows that a_4 is independent of F (the so-called saturation phenomenon) and is proportional to $1/g_{24}$. Moreover, equations (21) and (22) show that the controller

response amplitude a_2 is also independent of F. This phenomenon is different from the 1:2 non-linear vibration absorber (see equation (1)), where the controller response amplitude is proportional to $\sqrt{F}$ [7].

If $g_2 = 0$ and $\zeta_2 = \Omega - 2\omega_2 = 0$, it follows from equations (22), (17), and (18) that

$$a_4 = 0, \qquad a_1 = \left(\frac{8F}{|g_1|\omega_1^2}\right)^{1/4}. \tag{28}$$

It shows that a_1 can be controlled by changing g_1 and is proportional to $F^{1/4}$. Hence, when the excitation amplitude F increases, the additional excitation energy is guided to the controller u_1 instead of the controller u_2.

It follows from equation (25) that

$$g_1 u_1^2 \dot{u}_1^2 = \frac{g_1 a_1^4}{8}\left(\frac{\Omega}{4}\right)^2 [1 - \cos(\Omega t - (\phi_1 - \phi_2 + 2\phi_4))]. \tag{29}$$

One can see from equations (15) and (16) that, when $a_2 \neq 0$ and $\zeta_2 = 0$, $\phi_2 = 0^\circ$ (if $\Omega < 2\omega_2$) or 90° (if $\Omega = 2\omega_2$) or 180° (if $\Omega > 2\omega_2$). Also, it follows from equations (13) and (14) that, when $a_1 \neq 0$, $\zeta_1 = 0$, and $g_{124} > 0$, $\phi_4 = 0^\circ$ (if $\Omega < 4\omega_1$) or 90° (if $\Omega = 4\omega_1$) or 180° (if $\Omega > 4\omega_1$). Moreover, when $a_1 \neq 0$, $\zeta_1 = 0$, and $g_{124} < 0$, $\phi_4 = 180^\circ$ (if $\Omega < 4\omega_1$) or -90° (if $\Omega = 4\omega_1$) or 0° (if $\Omega > 4\omega_1$). Furthermore, it follows from equations (17) and (18) that, if $g_2 = 0$, $g_1 < 0$, $\Omega \neq 4\omega_1$, and a_4 is small and negligible, $\phi_1 = 180^\circ$ (if $\Omega < 2\omega_2$) or -90° (if $\Omega = 2\omega_2$) or 0° (if $\Omega > 2\omega_2$). Moreover, if $g_2 = 0$, $g_1 < 0$, $\Omega = 4\omega_1$, and a_4 is small and negligible, $\phi_1 = 0^\circ$ (if $\Omega < 2\omega_2$) or 90° (if $\Omega = 2\omega_2$) or 180° (if $\Omega > 2\omega_2$). Hence $\phi_1 - \phi_2 + 2\phi_4 = \pm 180^\circ$ if $g_1 < 0$, and it follows from equations (29) and (28) that

$$g_1 u_1^2 \dot{u}_1^2 = -F - F\cos\Omega t, \tag{30}$$

where $\Omega/4$ is replaced with ω_1. It shows that $g_1 u_1^2 \dot{u}_1^2$ has a harmonic component to cancel the external excitation force and a static component to make $u_4 = -F/\omega_4^2$. This phenomenon is exactly the same as the saturation phenomenon in the 1:2 non-linear vibration absorber. However, here the controller frequency (i.e., ω_1) is equal to $\Omega/4$ instead of $\Omega/2$, and a quartic term is used instead of a quadratic term.

4. NUMERICAL AND EXPERIMENTAL RESULTS

Figure 2 shows the cantilevered skew plate with the 1:2:4 non-linear vibration absorber designed for controlling the first-mode vibration of the plate. An attempt to use the plate velocity measured by the scanning laser vibrometer to provide the required velocity feedback (see equation (5)) was not successful. The signal from the laser vibrometer is sent through an analog filter before it is digitized. Because of the analog filtering, the phase difference between the velocity signal from the laser vibrometer and the displacement signal from the PZT sensor is not 90°. Hence, we use the numerical time derivative $v4$ (i.e., $\dot{u}_4$) shown in Figure 2 to provide the required velocity feedback from the plate. We note that there is no filter used in this vibration absorber because the numerical time derivative filters out the constant offset inherent in the measured voltage due to the interaction between the PZT sensor and the DSP board. This constant offset forced us to use a band-pass filter in the 1:2 vibration absorber, as shown in Figure 1. Although high-frequency noise may be

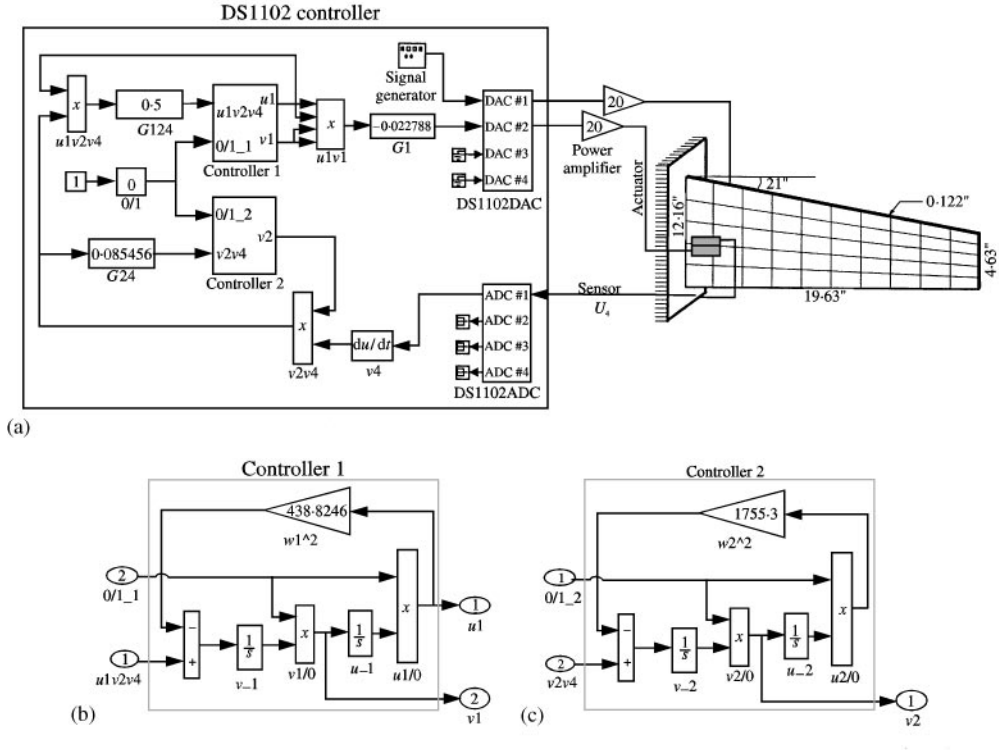

Figure 2. Experimental set-up for controlling the first-mode vibration: (a) the plate with the 1 : 2 : 4 non-linear vibration absorber, (b) the subsystem "Controller 1", and (c) the subsystem "Controller 2".

magnified by the numerical time derivative, it does not affect this 1 : 2 : 4 vibration absorber because its frequency is well above those of the controllers. One can follow the procedure used in deriving equation (4) to obtain from Figure 2 that

$$\ddot{u}_1 + \omega_1^2 u_1 = G124 \times u_1 \dot{u}_2 \dot{u}_4, \qquad \ddot{u}_2 + \omega_2^2 u_2 = G24 \times \dot{u}_2 \dot{u}_4,$$

$$10{\cdot}85(\ddot{u}_4 + 0{\cdot}5028\dot{u}_2 + 7021u_2) = \frac{F}{\hat{F}}[G1 \times 200u_1^2\dot{u}_1^2 + \hat{F}\cos(\Omega t)]. \tag{31}$$

Equations (21) and (22) show that setting $\zeta_1 = \zeta_2 = 0$ reduces a_4. Moreover, it will be shown in section 5 that, when both g_1 an g_2 are used, g_2 will dominate the control and this 1 : 2 : 4 vibration absorber will behave almost the same as the 1 : 2 vibration absorber. Hence, we only consider the case that $\zeta_1 = \zeta_2 = g_2 = 0$ in equation (31).

To perform numerical simulation of equation (31) we built the SIMULINK model shown in Figure 3, where the subsystems "controller 1" and "controller 2" are those shown in Figures 2(b) and 2(c). The gain $G1$ in Figure 3 contains the factor 200 due to the power amplifier and the scaling factor 10 of the DSP output. In the numerical simulation, the ordinary differential equation solver selected is the MATLAB fixed-step solver ode4, which uses a fourth-order Runge–Kutta integration method. The integration step size is 0·005 s. The parameters used in the SIMULINK solution are also used in performing the real-time control. For the numerical simulation and experiments the following parameters are chosen

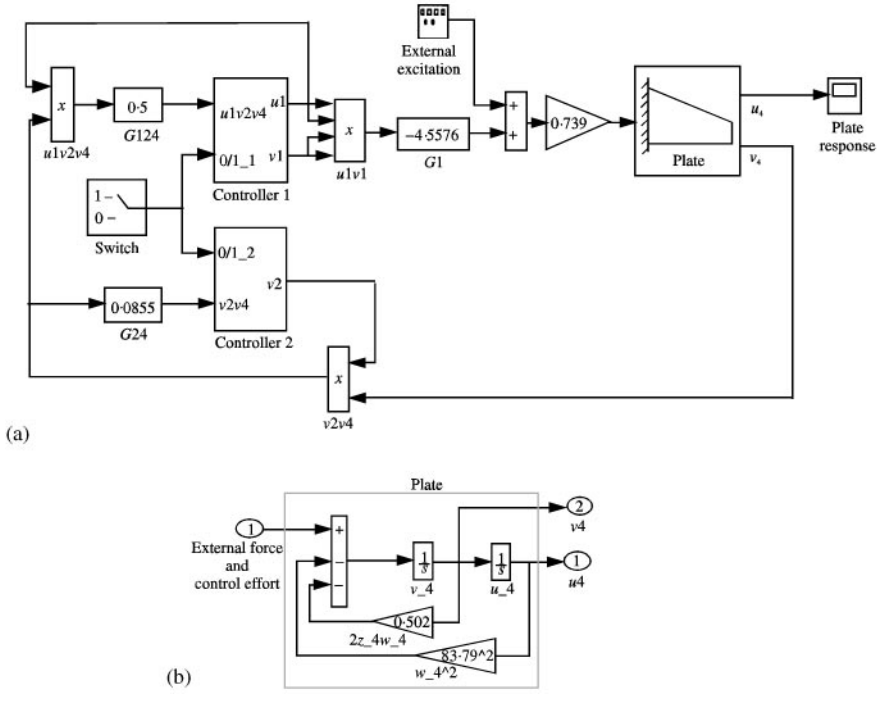

Figure 3. The SIMULINK model for numerical simulation of the first-mode control (a) the plate with the 1:2:4 non-linear vibration absorber, and (b) the subsystem "Plate".

based on the limitations of the PZT patches for actuation and the dSPACE controller system:

$$G124 = 0{\cdot}5, \qquad G24 = \frac{300}{\omega_2\omega_4}, \qquad G1 = \frac{-10}{\omega_1^2}, \qquad \hat{F} = 10\ \text{V},$$

$$\Omega = 2\omega_2 = 4\omega_1, \qquad g_2 = \zeta_1 = \zeta_2 = 0. \tag{32}$$

Moreover, the initial conditions are chosen to be $u_1 = u_2 = 0{\cdot}1$, $\dot{u}_1 = \dot{u}_2 = 0$, and $u_4 = \dot{u}_4 = 0$.

Figure 4 shows the sensor response u_4 and the controller responses u_1 and u_2 in controlling the first-mode steady-state vibration. The experimental result shown in Figure 4(a) is obtained by exciting the plate using $10\cos(\omega_4 t)$ V to the QP10W patch on the backside of the plate. The controller is turned on about 5 s after data collection is started. The experimental results agree closely with the numerical results. The transient effects in the experimental sensor response u_4 and controller response u_1 are similar to those in the numerical responses. The time to reach a steady-state after the controller is activated is almost the same, and the experimental steady-state values of u_1 and u_4 are the same as the numerical ones. However, the steady-state controller response u_2 in the experiment is different from that in the numerical simulation because $\zeta_1 = \zeta_2 = 0$ and $\Omega = 2\omega_2 = 4\omega_1$ (see equation (32)) and hence a_2 is undetermined and depends on initial conditions, as explained in section 3.1.

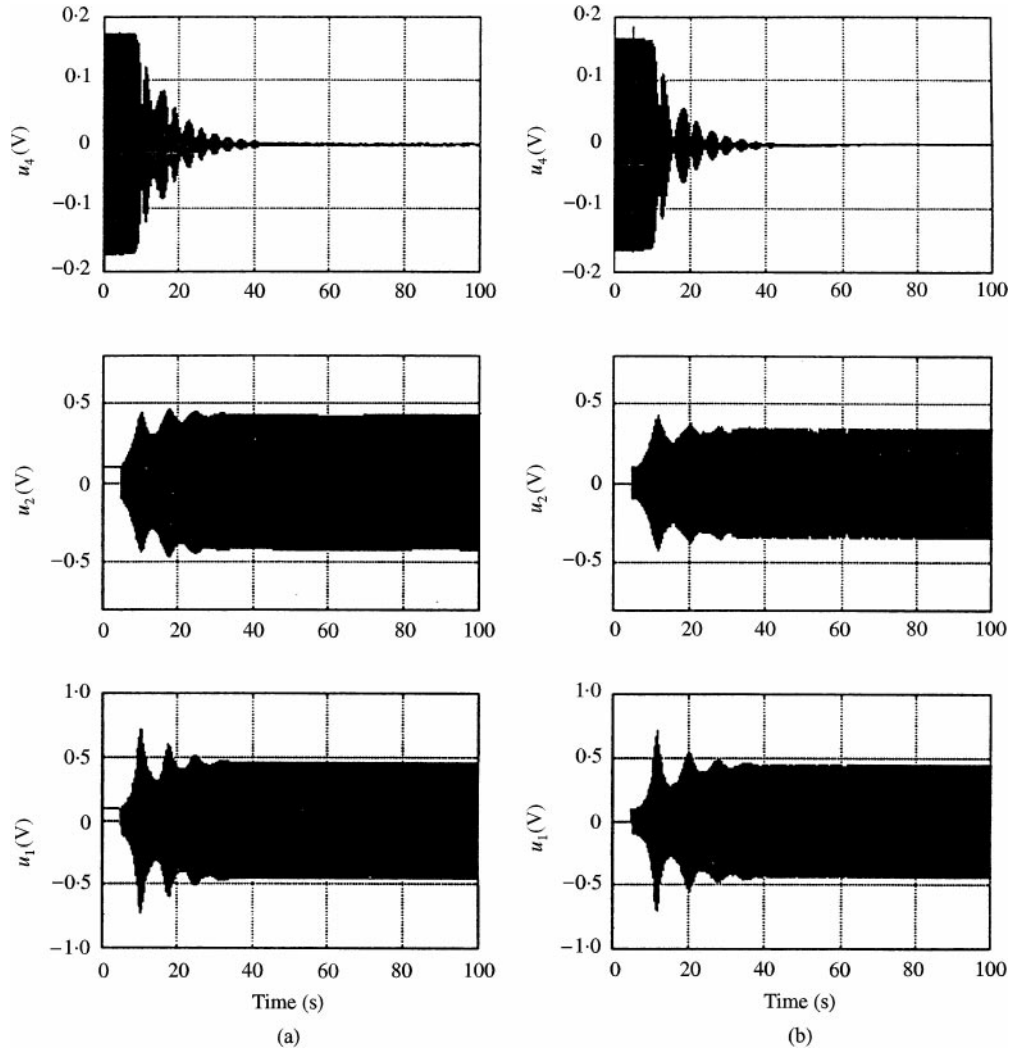

Figure 4. The sensor response u_4 and controller responses u_1 and u_2 in controlling the first-mode vibration: (a) experimental results, and (b) numerical results using equations (31) and (32).

The force response curves shown in Figure 5 reveal the saturation phenomenon of this new 1 : 2 : 4 non-linear vibration absorber. The experimental and numerical values of a_4 are very close to zero and are independent of the external excitation amplitude F. The perturbation analysis predicts a_4 to be zero, as shown in equation (28). The controller response amplitude a_1 follows the perturbation solution shown in equation (28). Again the experimental controller amplitude a_2 in Figure 5 deviates from the numerical one because it depends on initial conditions. It is difficult to control the initial conditions because they are determined by the time that the controllers are activated and the phase of u_4 at that specific time. This also explains why the u_2 in Figure 4(a) is different from that in Figure 4(b). When $a_4 \neq 0$ and $\zeta_1 \neq 0$ and/or $\Omega \neq 4\omega_1$, numerical and experimental results show that the steady-state value of a_2 is determinant and constant, as predicted by equation (21).

The experimental time traces shown in Figure 6 verify the perturbation prediction shown in equation (30). It shows that $g_1 u_1^2 \dot{u}_1^2$ has a harmonic component to cancel out the external

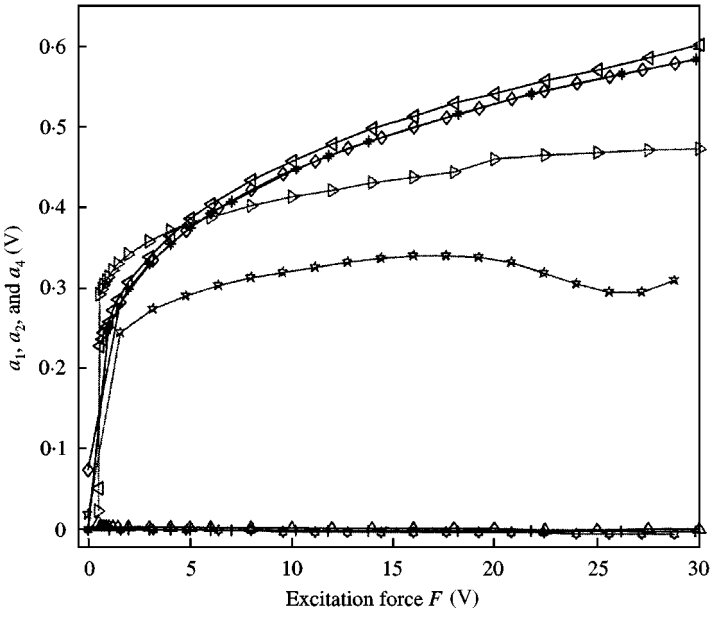

Figure 5. The numerical and experimental forces response curves. Experiment: ◁, a_1; ▷, a_2; △, a_4. Numerical: ◇, a_1; ★, a_2; ☆, a_4. perturbation: ∗, a_1; +, a_4.

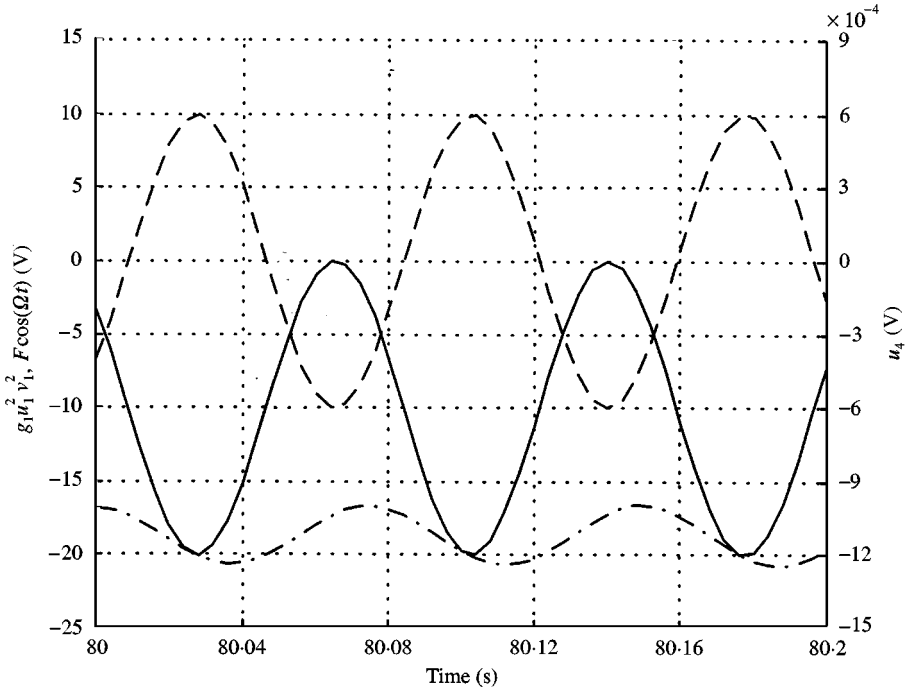

Figure 6. The relationship between the controller output $g_1u_1^2\dot{u}_1^2$, the excitation force $F\cos(\Omega t)$, and the plate response u_4: ——, $g_1u_1^2\dot{u}_1^2$; – – –, $F\cos(\Omega t)$; – · –, u_4.

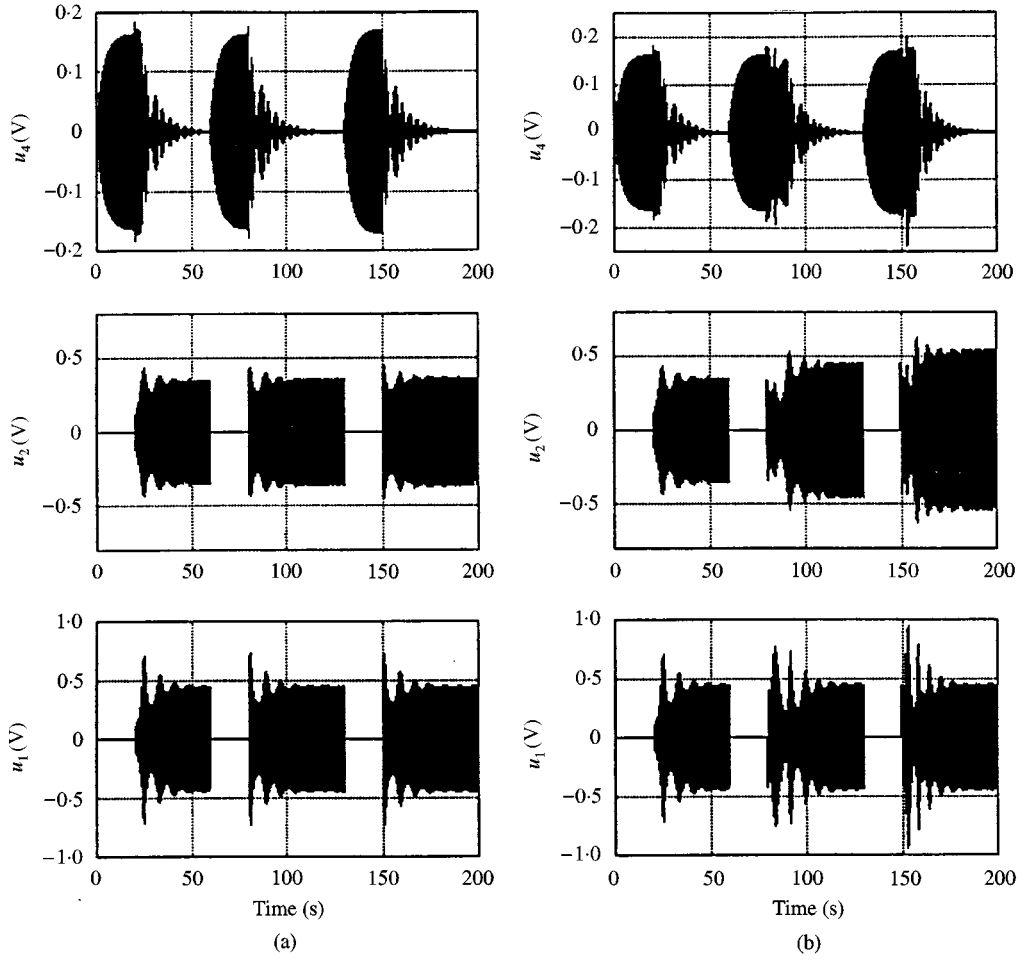

Figure 7. Numerical simulation of the 1:2:4 non-linear vibration absorber in controlling the first-mode vibration by using equations (31) and (32) with the controllers being on and off at: (a) one time sequences, and (b) another time sequences.

harmonic excitation and a static component to make $u_4 = -F/\omega_4^2$. Using $F = 10 \times 0{\cdot}739 = 7{\cdot}39$ we obtain $u_4 = -0{\cdot}0011$, which is equal to the mean value of u_4 in Figure 6.

Figure 7 shows the robustness of this 1:2:4 non-linear vibration absorber in controlling the first-mode steady-state vibration. Figures 7(a) and 7(b) show numerical results obtained using the same parameters but different time sequences for the activation and deactivation of the controllers. In Figure 7(a), the plate vibration u_4 is always immediately suppressed after the controllers are activated. When the plate vibration u_4 reaches its steady-state, the controller responses u_2 and u_1 also settle at their steady-state values. Figure 7(b) shows that different initial conditions may cause different transient effects, but u_4 is always suppressed to zero and u_1 always settles at the same steady-state value. However, the controller response u_2 does not settle at the same value because of different initial conditions, as explained in section 3.1.

Figure 8 shows the experimental verification of the robustness of this 1:2:4 non-linear vibration absorber in controlling the first-mode steady-state vibrations. Figure 8(a) verifies

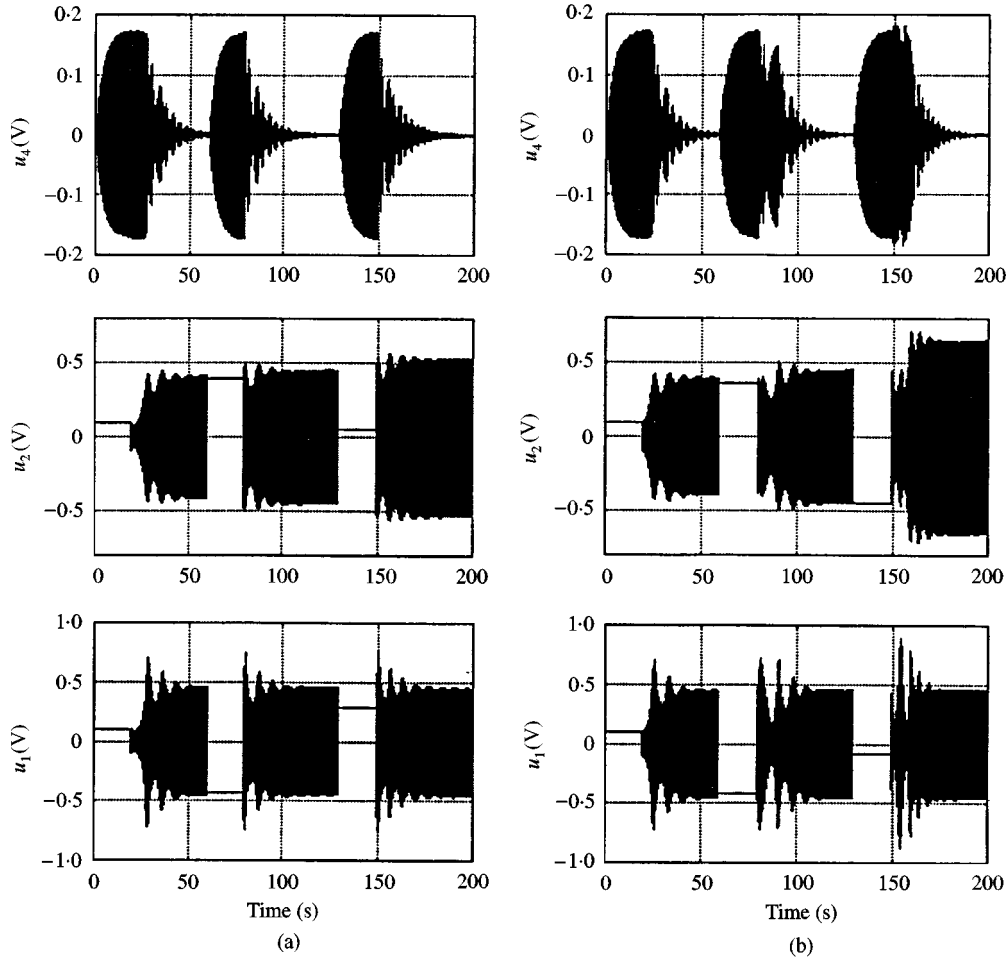

Figure 8. Experimental results of the 1:2:4 non-linear vibration absorber in controlling the first-mode vibration with the controllers being on and off at the same time sequences: (a) the first run, and (b) the second run.

the numerical results shown in Figure 7(a). Figure 8(b) was obtained using the same settings used in Figure 8(a). After collecting data for Figure 8(a) the controller was reset and the C-code for the model shown in Figure 2 was regenerated in an attempt to repeat and verify the results in Figure 8(a). However, the controller response u_2 in Figure 8(b) is different from that in Figure 8(a) because the initial conditions cannot be controlled to be the same. Figures 7 and 8 show that this 1:2:4 vibration absorber is more sensitive to initial conditions than the 1:2 vibration absorber.

5. OTHER HIGHER-ORDER NON-LINEAR VIBRATION ABSORBERS

With the understanding of the 1:2 non-linear vibration absorber [7, 8], we designed and examined several vibration absorbers using different orders of non-linearities and internal resonances before the design of the 1:2:4 non-linear vibration absorber shown in equation (5). Some of these vibration absorbers deserve attention.

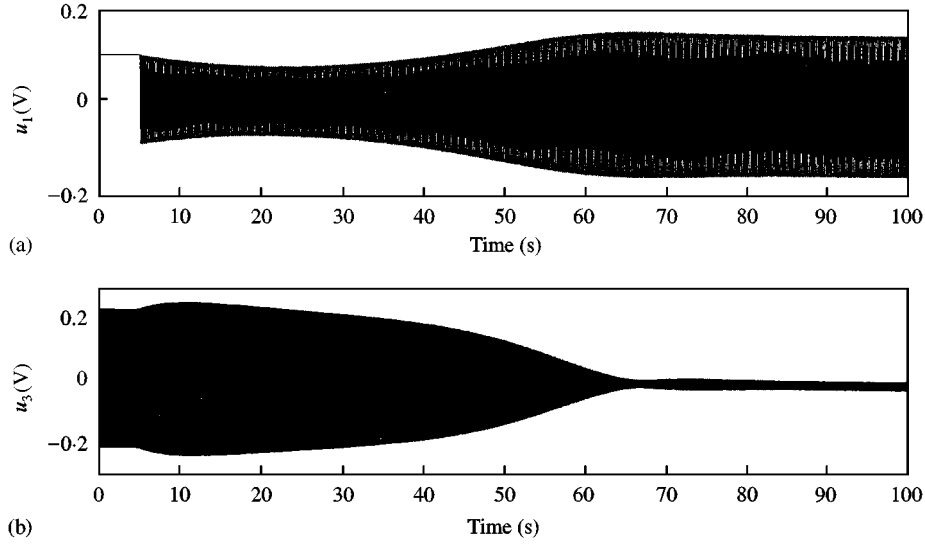

Figure 9. Numerical simulation of the 1 : 3 vibration absorber shown in equation (33) with u_1 activated at $t = 5$ s: (a) u_1, and (b) u_3.

First, we studied a 1 : 3 vibration absorber, which was designed to be

$$\ddot{u}_1 + 2\zeta_1\omega_1\dot{u}_1 + \omega_1^2 u_1 = g_{13}u_1^2 u_3,$$
$$\ddot{u}_3 + 2\zeta_3\omega_3\dot{u}_3 + \omega_3^2 u_3 = g_1 u_1^3 + F\cos(\Omega t). \tag{33}$$

Figure 9 shows the responses obtained using $g_{13} = 300$, $g_1 = 7960$, $F = 7{\cdot}96$, $\zeta_1 = 0$, $\zeta_3 = 0{\cdot}0025$, and $\Omega = \omega_3 = 3\omega_1 = 82{\cdot}5$ rad/s. Because the control force $g_1 u_1^3$ does not provide a constant term as a 1 : 2 vibration absorber does (see equation (30)), the transient effect can be significant and depends on initial conditions, which are determined by the activation time of the the controller.

To reduce the controlled amplitude of u_3 in Figure 9 we designed the following vibration absorber:

$$\ddot{u}_1 + 2\zeta_1\omega_1\dot{u}_1 + \omega_1^2 u_1 = g_{13}u_1\dot{u}_1\dot{u}_3,$$
$$\ddot{u}_3 + 2\zeta_3\omega_3\dot{u}_3 + \omega_3^2 u_3 = g_1 u_1^3 + F\cos(\Omega t). \tag{34}$$

The response obtained using $g_{13} = 300/\omega_1\omega_3$, $g_1 = 7960$, $F = 7{\cdot}96$, $\zeta_1 = 0$, $\zeta_3 = 0{\cdot}0025$, and $\Omega = \omega_3 = 3\omega_1 = 82{\cdot}5$ rad/s shows that the use of velocity feedback $\dot{u}_3$ reduces the controlled vibration amplitude of u_3. In an intend to reduce the transient period in Figure 9, a quadratic term was added and $g_1(u_1^3 + u_1^2)$ was used in equation (34). However, it did not work well because u_1^2 adds another excitation harmonic to the system. Hence, we consider the following 1 : 4 vibration absorber:

$$\ddot{u}_1 + 2\zeta_1\omega_1\dot{u}_1 + \omega_1^2 u_1 = g_{14}u_1^2\dot{u}_1\dot{u}_4,$$
$$\ddot{u}_4 + 2\zeta_4\omega_4\dot{u}_4 + \omega_4^2 u_4 = g_1 u_1^4 + F\cos(\Omega t). \tag{35}$$

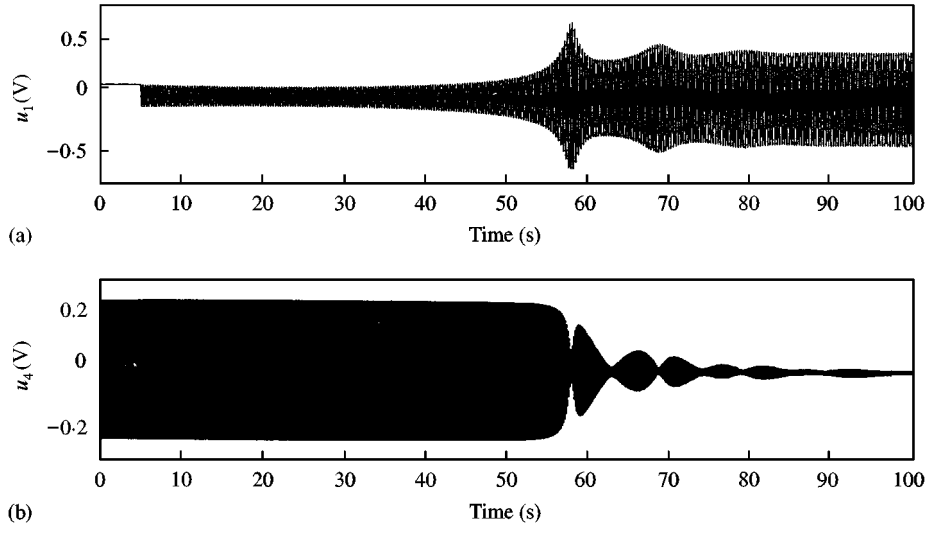

Figure 10. Numerical simulation of the 1:4 vibration absorber shown in equation (35) with $u_1(0) = 0{\cdot}1$: (a) u_1, and (b) u_4.

Figure 10 shows the response obtained using $g_{14} = 2$, $g_1 = 2000$, $F = 7{\cdot}96$, $\zeta_1 = 0$, $\zeta_4 = 0{\cdot}0025$, and $\Omega = \omega_4 = 4\omega_1 = 82{\cdot}5$ rad/s. Figures 10(a) and 10(b) show that, if the initial condition $u_1(0)$ is set to be too small, it takes a long time for u_1 to grow to suppress u_4 because of the use of u_1^4. Because u_1^4 contains a $2\omega_1$ − harmonic, it causes the non-zero amplitude of u_4. Hence, we improve this vibration absorber as

$$\begin{aligned} &\ddot{u}_1 + 2\zeta_1\omega_1\dot{u}_1 + \omega_1^2 u_1 = g_{14}u_1^2\dot{u}_1\dot{u}_4, \\ &\ddot{u}_4 + 2\zeta_4\omega_4\dot{u}_4 + \omega_4^2 u_4 = g_1 u_1^2\dot{u}_1^2 + F\cos(\Omega t). \end{aligned} \tag{36}$$

The response obtained using $g_{14} = 2$, $g_1 = -2000/\omega_1^2$, $F = 7{\cdot}96$, $\zeta_1 = 0$, $\zeta_4 = 0{\cdot}0025$, and $\Omega = \omega_4 = 4\omega_1 = 82{\cdot}5$ rad/s show that the use of $u_1^2\dot{u}_1^2$ (instead of u_1^4) reduces u_4. However, the problem of having a long transient period when $u_1(0)$ is small still exists. Hence, we design the following 1:2:4 vibration absorber:

$$\begin{aligned} &\ddot{u}_1 + 2\zeta_1\omega_1\dot{u}_1 + \omega_1^2 u_1 = g_{124}u_1\dot{u}_2\dot{u}_4, \qquad \ddot{u}_2 + 2\zeta_2\omega_2\dot{u}_2 + \omega_2^2 u_2 = g_{24}\dot{u}_2\dot{u}_4, \\ &\ddot{u}_4 + 2\zeta_4\omega_4\dot{u}_4 + \omega_4^2 u_4 = g_1 u_1^2\dot{u}_1^2 + F\cos(\Omega t). \end{aligned} \tag{37}$$

Figure 11 shows the responses obtained using $g_{124} = 2$, $g_{24} = 300/\omega_2\omega_4$, $g_1 = -2000/\omega_1^2$, $F = 7{\cdot}96$, $\zeta_1 = \zeta_2 = 0$, $\zeta_4 = 0{\cdot}0025$, and $\Omega = \omega_4 = 2\omega_2 = 4\omega_1 = 82{\cdot}5$ rad/s. One can see from Figure 11(a,c) and Figures 10(a,b) that the inclusion of the controller u_2 significantly reduces the transient period. Moreover, Figure 11(d) shows the static component of u_4 caused by the static force predicted by the perturbation solution shown in equation (30).

To understand the influence of u_1 on u_2 and u_4, we consider

$$\begin{aligned} &\ddot{u}_1 + 2\zeta_1\omega_1\dot{u}_1 + \omega_1^2 u_1 = g_{124}u_1\dot{u}_2\dot{u}_4, \qquad \ddot{u}_2 + 2\zeta_2\omega_2\dot{u}_2 + \omega_2^2 u_2 = g_{24}\dot{u}_2\dot{u}_4, \\ &\ddot{u}_4 + 2\zeta_4\omega_4\dot{u}_4 + \omega_4^2 u_4 = g_2 u_2^2 + F\cos(\Omega t). \end{aligned} \tag{38}$$

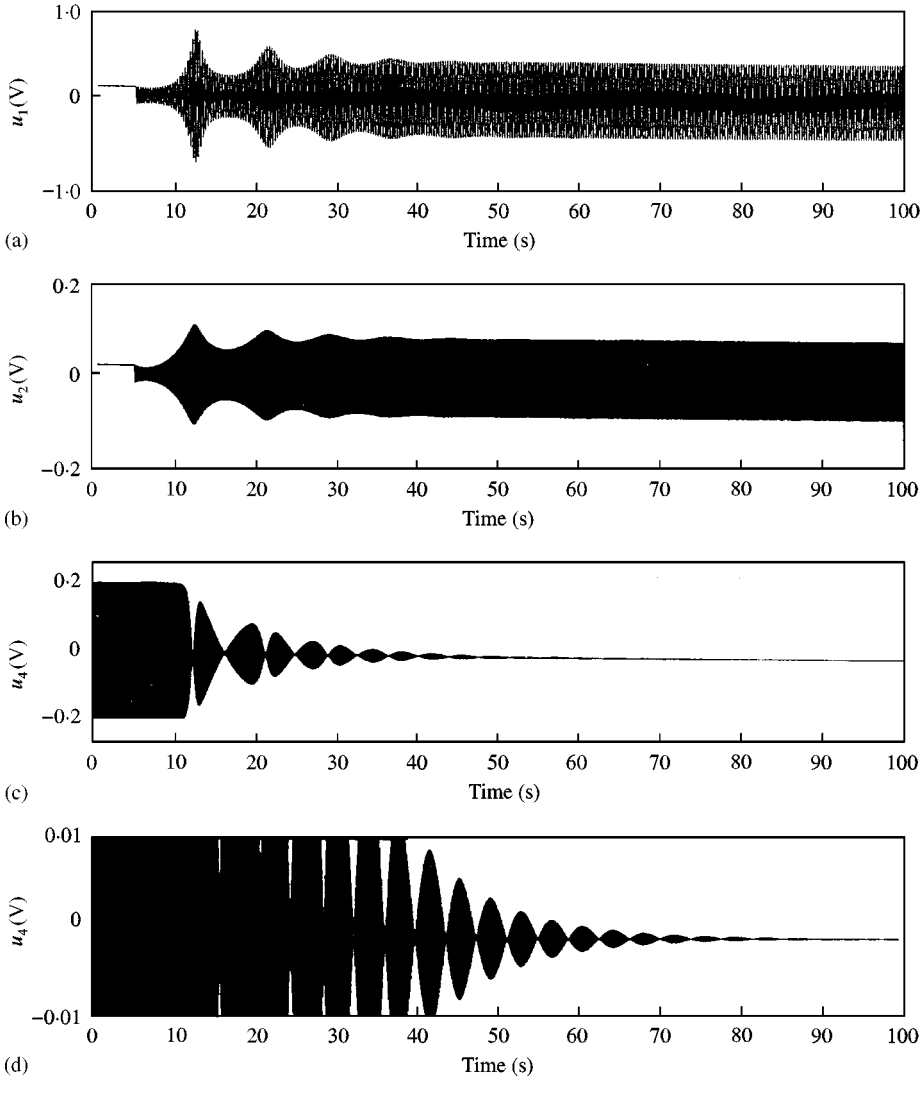

Figure 11. Numerical simulation of the 1:2:4 vibration absorber shown in equation (37): (a) u_1, (b) u_2, (c) u_4, and (d) u_4.

The response obtained using $g_{124} = 2$, $g_{24} = 300/\omega_2\omega_4$, $g_2 = 7960$, $F = 7{\cdot}96$, $\zeta_1 = 0{\cdot}002$, $\zeta_2 = 0$, $\zeta_4 = 0{\cdot}0025$, and $\Omega = \omega_4 = 2\omega_2 = 4\omega_1 = 82{\cdot}5$ rad/s shows that u_2 is not influenced by u_1 and u_1 dies out because $\zeta_1 \neq 0$ and u_1 does not directly interact with u_2 or u_4.

If $g_2u_2^2$ is added to equation (37) as shown in equation (5), the response obtained using $g_{124} = 2$, $g_{24} = 300/\omega_2\omega_4$, $g_1 = -2000/\omega_1^2$, $g_2 = 7960$, $F = 7{\cdot}96$, $\zeta_1 = \zeta_2 = 0$, $\zeta_4 = 0{\cdot}0025$, and $\Omega = \omega_4 = 2\omega_2 = 4\omega_1 = 82{\cdot}5$ rad/s reveals that the response is mainly controlled by u_2 because u_2 grows faster than u_1 after they are activated.

6. CONCLUDING REMARKS

The use of PZT patches and higher-order saturation phenomena to suppress the steady-state resonant vibrations of a cantilevered skew aluminium plate is shown by

perturbation analysis, numerical simulation, and experiments. Several new non-linear vibration absorbers are studied. A new 1 : 2 : 4 non-linear vibration absorber is designed and examined in detail. Numerical and experimental results show the feasibility and robustness of this new non-linear vibration absorber.

ACKNOWLEDGMENT

This work is supported by the U.S. Army Research Office through Grant DAAH04-96-1-0048 and is partially supported by the National Science Foundation through Grant CMS-9871288. This support is gratefully acknowledged.

REFERENCES

1. A. H. NAYFEH and D. T. MOOK 1979 *Nonlinear Oscillations*. New York: Wiley.
2. M. F. GOLNARAGHI 1991 *Journal of Dynamics and Control* **1**, 405–428. Regulation of flexible structures via nonlinear coupling.
3. S. S. OUEINI, A. H. NAYFEH and M. F. GOLNARAGHI 1997 *Nonlinear Dynamics* **13**, 189–202. A theoretical and experimental implementation of a control method based on saturation.
4. S. S. OUEINI, A. H. NAYFEH and J. PRATT 1998 *Nonlinear Dynamics* **15**, 259–282. A nonlinear vibration absorber for flexible structures.
5. J. PRATT and A. H. NAYFEH 1997 *38th AIAA Structures, Structural Dynamics, and Materials Conference, Kissimmee*, FL. Active vibration control for chatter suppression.
6. S. S. OUEINI and A. H. NAYFEH 1997 *38th AIAA Structures, Structural Dynamics, and Materials Conference, Kissimmee, FL*. Multimode control of flexible structures using saturation.
7. P. F. PAI, B. WEN, A. S. NASER and M. J. SCHULZ 1998 *Journal of Sound and Vibration* **215**, 273–296. Structural vibration control using PZT patches and nonlinear phenomena.
8. P.F. PAI and M. J. SCHILZ 2000 *International Journal of Mechanical Sciences* **42**, 537–560. A refined nonlinear vibration absorber.
9. P. F. PAI, *GESA* (*Geometrically Exact Structural Analysis*): *A finite element code for analyzing highly flexible structures*, Department of Mechanical and Aerospace Engineering, University of Missouri-Columbia, Columbia, MO, 1999.
10. P. F. PAI, B. ROMMEL and M. J. SCHULZ 1999 *The SPIE Smart Structures and Materials'99, Newport Beach, CA*. Structural vibration suppression using PZT patches and higher-order saturation phenomena.
11. P. F. PAI and A. H. NAYFEH 1991 *Nonlinear Dynamics* **2**, 1–34. Three-dimensional nonlinear vibrations of composite beams—II. Flapwise excitations.